Amplification regimes of the orotron: A single-resonator amplifier

D. M. Vavriv[1] and K. Schünemann[2]
[1]*Radio Astronomy Institute of Ukrainian Academy of Sciences, 4 Chervonopraporna Street, 310002 Kharkov, Ukraine*
[2]*Technical University Hamburg–Harburg, Arbeitsbereich Hochfrequenztechnik, Wallgraben 55, D-21071 Hamburg, Germany*
(Received 12 August 1997; revised manuscript received 7 January 1998)

A self-consistent, nonlinear model of orotron amplifiers is proposed for investigating single-stage and multistage amplifiers. The single-resonator amplifier is studied in detail including linear and nonlinear modes of amplification. A comparative study of both collective and single-electron interaction regimes is performed. The fundamentals which determine the level of amplifier performance are identified, and limiting output characteristics of the amplifier are determined. The theoretical results are compared with experimental data known to date. [S1063-651X(98)02605-1]

PACS number(s): 41.60.−m

I. INTRODUCTION

The orotron, which is now recognized as an effective source of electromagnetic radiation through the millimeter and submillimeter wavelength bands, was introduced by Rusin and Bogomolov in 1966 [1]. Several versions of orotron type devices, referred to as diffraction radiation generator [2], ledatron [3], Smith-Purcell free-electron laser [4], and planar orotron [5], have also been developed and tested. The advantages of the orotron result from both the use of an open resonator with a diffraction grating as an oscillatory system, and the exploitation of the Smith-Purcell radiation [6], which is a kind of Cerenkov radiation, for resonator excitation. The beam-field interaction in the orotron combines peculiarities, which are inherent both in resonance generators, like the klystron, and nonresonance devices with distributed interaction, like the traveling wave tube.

Orotron research activities have mainly concentrated on the development of autogenerators. The physics of their operation is well understood, and adequately described due to efforts of a number of researchers (see, e.g., Refs. [1–14]). In practice, the most popular orotron design is that with a semispherical open resonator containing a grating on the plane mirror and a ribbonlike beam skimming over the grating. Such tubes provide tens of watts at the output in an 8-mm wavelength band, and several watts in a 3-mm band with electron beams of a relatively low energy of 3 kV and a beam current of about 100 mA [14].

It was also clear from the very first orotron experiments, and from theoretical studies [8,15,16], that the amplification mode of operation can be realized under some specific conditions. The results of experimental investigations reported up to now [17,18] have demonstrated the amplification effect in the orotron. These amplifiers have been built on the basis of the above mentioned oscillatory system (see Fig. 1), with approximately the same values of the beam voltage and current. However, progress in amplifier research is moderate compared to that for generators, both in the development of practical amplifiers and in theoretical studies. So far the amplifier output characteristics in general do not meet practical needs. The theoretical results on record do not provide clear answers to questions like the following: It is possible to improve the output characteristics of these amplifiers? What is the optimal design? What are the potentialities of orotron-type amplifiers? The aim of our study is to provide answers to these questions through the analysis of small- and large-signal amplification modes of the orotron for both single-electron and collective regimes of the electron-wave interaction. In this paper, we derive a unified self-consistent mathematical model which is suitable to study both single-resonator and multiresonator amplifiers, as illustrated in Figs. 1 and 2. We then apply this model for studying the single-resonator amplifier in sufficient detail.

Our analysis is based on the solution of a set of self-consistent equations including Maxwell's equations, the Poisson equation for the space charge field, and the equation of particle motion. To simplify these equations, we use approaches which have generally been accepted in the theory of orotron oscillators. The most important of them are the following: We assume that a single high-Q mode is excited in the resonator, and that the motion of particles follows a straight line. We restrict ourselves to the case of a nonrelativistic, monoenergetic electron beam.

When deriving the final equations, we intensively use the fact that there are three characteristic time scales which essentially differ in magnitude, namely, the field period, the transient time of electrons through the resonator, and the relaxation time of the resonator field. This allows us, as in the case of other resonance devices like lasers, magnetrons, and gyrotrons (see, e.g., Refs. [19–22], first to use an aver-

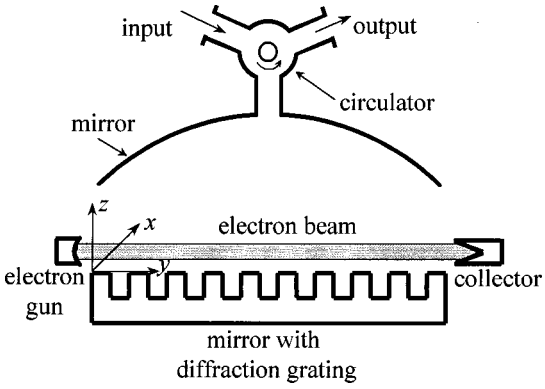

FIG. 1. Schematic of a single-resonator orotron amplifier with the coordinate system chosen.

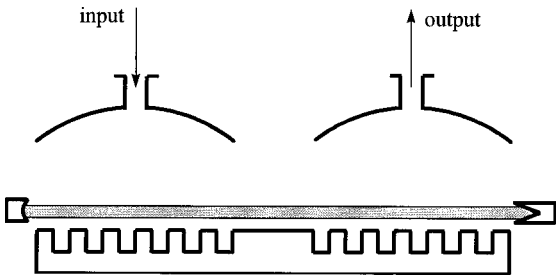

FIG. 2. Schematic of a two-stage orotron amplifier.

aging technique which eliminates the fast-time-scale phenomena, and next to account for the effect of the electron beam on the resonator field dynamics through the introduction of some integral characteristics. Depending upon a specific set of control parameters, the proposed model describes self-running oscillations, synchronization of the orotron oscillation, and various regimes of amplification.

The paper is organized as follows. The basic equations are given in Sec. II. The description of the field structure in an open resonator, the derivation of the equations of resonator excitation, the equation of motion, and the space charge representation, which are given in Secs. II A, II B, II C, and II D, respectively, should be considered as a brief review of methods and approaches usually used in orotron studies. In Sec. II D, the final system of equations is described. Section III deals with the analysis of the single-resonator amplifier. It includes small- and large-signal analyses, a stability analysis, a comparative study of collective and single-electron interaction regimes, and a comparison of theoretical and experimental results. Section IV contains discussion of results and conclusions.

II. BASIC EQUATIONS

To study the physics of orotron amplifiers and to calculate their characteristics, we will derive a set of equations self-consistently, describing the interaction of an electron beam with the electromagnetic field inside any of the resonators of a multistage orotron amplifier. The mathematical model for the single-resonator amplifier depicted in Fig. 1 will then be obtained as a limit of this approach.

A. Resonator field

Provided that each of the resonators supports a single high-Q mode, the field excited in any of the amplifier resonators can be written in the following form [22]:

$$\vec{E}=\mathrm{Re}\{\vec{E}_r(\vec{r})C(t)e^{-i\omega t-i\gamma(t)}-\mathrm{grad}\ \phi\}. \tag{1}$$

Here $\vec{E}_r(\vec{r})$ is the spatial distribution of a resonator mode, and $C(t)$ and $\gamma(t)$ are the amplitude and phase of the mode, respectively, which are in general slowly varying functions of time compared to the function $\exp(-i\omega t)$. ω is the frequency of an external signal which is considered to be close to the natural frequency ω_r of a resonator mode, and the term grad φ describes the space charge field of an electron beam. φ is the field potential.

Because of the presence of a grating, the resonator field contains an infinite number of space harmonics, including that propagating in a direction nearby perpendicular to the grating, and slow waves which are localized in its vicinity. Provided that the grating period l and the wavelength $\lambda \equiv 2\pi c/\omega$ (where c is the velocity of light) meet the condition $l \ll \lambda$, the y component of the resonator electric field, pointing in the direction of electron motion, may be approximated by the following expression [2]:

$$E_{ry}=A_0\Psi_s(x)\Psi_m(y)\left\{\sin[k_r(z-D)]+\sum_{\substack{n=-\infty\\ n\neq 0}}^{\infty}(a_n/a_0)\exp(-|\gamma_n|z+ik_ny)\right\}. \tag{2}$$

Here y is the beam axis; z is normal to the grating surface; x points along the grating ruling direction; A_0 is a normalized coefficient to be specified below; $k_r=\omega_r/c$; D is the distance between the resonator mirrors, which is assumed to be considerably smaller than curvatures of the mirrors; a_n/a_0 is the ratio of space harmonic amplitudes; k_n is the propagation constant along the grating of the nth harmonic, and $\gamma_n=\sqrt{k_r^2-k_n^2}$ is the constant of propagation along the z axis. $\Psi_s(x)$ and $\Psi_s(y)$ are functions describing the structure of the field, which corresponds to the structure of Gaussian beams:

$$\Psi_s(x)=\exp(-x^2/r_x^2)H_s(\sqrt{2}x/r_x),$$

$$\Psi_m(y)=\exp(-(y-L/2)^2/r_y^2)H_m(\sqrt{2}(y-L/2)/r_y), \tag{3}$$

where $H_s(\ )$ and $H_m(\ )$ are Hermite polynomials, r_x and r_y are the radii of the field spot on the grating in the x and y directions, and $y=0$, and $y=L/2$ correspond to the plane where the beam enters the resonator and to the resonator center, respectively. The sin term in Eq. (2) describes a standing wave formed due to reflections of the Smith-Purcell harmonic at the resonator mirrors. The summation is performed over all slow-wave harmonics, which are concentrated in a thin layer near the grating. The characteristic layer thickness is considered to be small compared to the mirror separation. The resonator mode described by Eq. (3) is usually denoted as quasi-TEM$_{smq}$ mode, where quasi stands for the perturbation introduced to the conventional field distribution in an open resonator by the grating, and s, m, and q are mode indexes.

Usually only a single slow wave, which is in space synchronism with the electrons, may exert a direct influence on electron motion. We define the wave with $n=1$ to be the synchronous one. Denoting this wave as E_{y1}, we can write its space distribution as follows:

$$E_{y1}(x,y,z)=A_0(a_1/a_0)\Psi_s(x)\times\exp(-|\gamma_1|z)\Psi_m(y)\exp(ik_1y), \tag{4}$$

where $k_1\approx 2\pi/l$. It should be emphasized that details of the function $f_y(y)\equiv\Psi_s(y)\exp(ik_1y)$ are of principal importance for orotron operation. To describe the corresponding effects, it is also convenient to use the Fourier presentation for this function:

$$f_y(y)=(2\pi)^{-1/2}\int_{-\infty}^{\infty} f_k(k)e^{iky}dk,$$

where $f_k(k)$ is the amplitude of the harmonic wave $\exp(iky)$, with k being the wave number. Introducing the intensity function $S_m(k)\equiv|f_k(k)|^2$, one can find

$$S_m(k)=(r_y^2/2)H_m^2(r_y(k-k_1)/\sqrt{2})\exp(-r_y^2(k-k_1)^2/2). \tag{5}$$

Thus the electrons experience a set of harmonics $\exp(iky)$ with continuous spatial spectrum. To set up equations governing the time evolution of the resonator field, we will self-consistently transform Maxwell's equations, the equation of particle motion, and the Poisson equation by taking into account the assumptions formulated above.

B. Equations of resonator excitation

To find equations for amplitude $C(t)$ and phase $\gamma(t)$, we first apply Maxwell's equations to the single-mode field given by Eq. (1), and next we eliminate fast varying terms by using the standard method of averaging [23]. Since this technique has been described in detail with respect to a number of resonance devices (see, e.g., Refs. [7, 9, 19–22]), we give only the final result, which in our case reads

$$\frac{dC}{dt}=-\frac{\omega_r}{2Q_r}C-\mathrm{Re}\left\{\frac{\exp(i\gamma)}{2N_r}\int_\sigma \vec{J}_1\cdot\vec{E}_r^{\,*}d\sigma\right\}+b_s\cos(\gamma-\varphi_s),$$

$$C\frac{d\gamma}{dt}=(\omega_r-\omega)C+\mathrm{Im}\left\{\frac{\exp(i\gamma)}{2N_r}\int_\sigma \vec{J}_1\cdot\vec{E}_r^{\,*}d\sigma\right\}-b_s\sin(\gamma-\varphi_s). \tag{6}$$

Here Q_r is the loaded Q factor of the excited mode, $N_r=\varepsilon_0\int_V\vec{E}_r\cdot\vec{E}_r^{\,*}dV$ is the mode norm with ε_0 the permittivity of free space, I_0 is the dc beam current, b_s is the amplitude of a possible external signal directly fed into the resonator, and t_0 is the moment at which an electron enters the resonator. Hence $t\equiv t(t_0,y)$ is considered as a function of both the entrance time t_0 and the distance y. When deriving these equations, the normalized coefficient A_0 in Eq. (2) was chosen as follows:

$$A_0=\left[2(a_1/a_0)\int_S\Psi_s(x)\Lambda(x,z)\exp(-|\gamma_1|z)dx\,dz\right]^{-1}, \tag{7}$$

where $\Lambda(x,z)$ determines the electron density distribution over the beam cross section S, obeying the following condition of normalization:

$$\int_S\Lambda(x,z)dx\,dz=1. \tag{8}$$

It should be pointed out that, specifying A_0, we remove an uncertainty in the definition of the norm N_r which includes A_0. In this case, N_r becomes dependent on the electron beam dimensions and the beam location inside the resonator as well as on the three-dimensional structure of the resonator field. To illustrate these dependencies, the norm is calculated in the Appendix.

As a final step in this section, we transform Eqs. (6) to a dimensionless form:

$$\frac{dF}{d\tau}=-F+\frac{G}{4\pi}\int_0^{\tilde{L}}\Psi_m(\xi)\int_0^{2\pi}\cos[\omega t(\varphi_0,\xi)-k_1r_y\xi+\gamma]d\varphi_0d\xi+A_s\cos\gamma,$$

$$\frac{d\gamma}{d\tau}=-\delta+\frac{G}{4\pi F}\int_0^{\tilde{L}}\Psi_m(\xi)\int_0^{2\pi}\sin[\omega t(\varphi_0,\xi)-k_1r_y\xi+\gamma]d\varphi_0d\xi-\frac{A_s}{F}\sin\gamma. \tag{9}$$

Here $\tau=t\omega/(2Q)$; $\xi=y/r_y$; $\varphi_0=\omega t_0$; $\tilde{L}=L/r_y$; $F=C/E_0$ is the normalized field strength with $E_0=U_0/r_y$; and $U_0=m\nu_0^2/2|e|$ is the value of the beam accelerating voltage, with ν_0 the initial velocity of the beam particles, and e and m the electron charge and mass, respectively. $G=2Qr_y^2I_0/(\omega_rN_rU_0)$ is the gain parameter or parameter of nonlinearity, $\delta=2Q(\omega_r-\omega)/\omega_r$ is the normalized frequency detuning, and $A_s=2Qb_s/(\omega_rE_0)$ is the normalized amplitude of the external force. It should be noted that the gain parameter G, introduced in Ref. [9], plays a principal role in the theory of the orotron. An example of its calculation and optimization is given in the Appendix. In order to find an equation for the function $t\equiv t(\varphi_0,\xi)$, which describes trajectories of the electrons we proceed to the equation of motion.

C. Motion equation

Under the assumption of a one-dimensional motion of the beam particles, their trajectory can be influenced by both the action of the y component of the electric field given in Eq. (4) and the space charge field of the beam. To take the effects of finite transverse dimensions of the beam into account, these fields are averaged over the beam cross section. Considering the normalization condition (7), we arrive at the following equation of motion:

$$\frac{d^2y}{dt^2}=\frac{e}{m}\left[\frac{1}{2}f_mC\cos(\omega t+\gamma-k_1y)+\overline{E}_{qy}\right], \tag{10}$$

where $\overline{E}_{qy}=\int_S\Lambda(x,y)E_{qy}(x,y,z)dxdy$ is the averaged y component of the space charge field.

Now let us rewrite the motion equation in Lagrange variables y and φ_0, with respect to

$$\Theta(\varphi_0,y)=\omega t(\varphi_0,y)-\varphi_0-\omega y/\nu_0, \tag{11}$$

which determines the variation of the electron phase under the action of both the resonator field and space charge waves. It is governed by

$$\frac{d^2\Theta}{d\xi^2}=\frac{\Phi_0}{2}\left(1+\frac{1}{\Phi_0}\frac{d\Theta}{d\xi}\right)^3 \times\left\{\frac{F}{2}\,\Psi_m(\xi)\cos(\Phi_s\xi+\Theta+\varphi_0+\gamma)+F_q\right\}. \tag{12}$$

Here $\Phi_0=\omega r_y/v_0$, $\Phi_s=\omega r_y(1/v_0-1/v_{\rm ph})$ is the velocity mismatch parameter with $v_{\rm ph}=\omega/k_1$, and $F_q=E_{qy}/E_0$ is the dimensionless strength of the beam space charge field.

The motion equation must be completed with initial conditions. If a nonmodulated beam enters a resonator, then

$$\Theta(\varphi_0,\xi)=d\Theta/d\xi=0 \quad \text{at } \xi=0 \quad \text{for } \varphi_0\in[0,2\pi]. \tag{13}$$

Such initial conditions are used for analyzing single-resonator amplifiers or the input stage of a multiresonator amplifier. For any next stage, the initial values of Θ and $d\Theta/d\xi$ are in general not equal to zero. In order to specify their values, it is previously necessary to solve the motion equation for electrons crossing the drift space, which separates the resonators.

D. Space charge field

Generally the space charge field is not a quasiharmonic but a quasiperiodic function of time. Hence it should be represented by a complete set of Fourier components,

$$E_{qy}=\mathrm{Re}\sum_{n=1}^{\infty}E_{qn}\exp(-in\omega t),$$

where E_{qy} is the complex amplitude of the nth harmonic of the y component of the space charge field. The harmonic amplitude E_{qn} is expressed in terms of the potential by $E_{qy}=-\partial\Phi_{en}/\partial y$, where the potential Φ_{en} of the nth harmonic obeys Poisson's equation

$$\nabla^2\Phi_{en}=-\rho_n/\varepsilon_0,$$

with the corresponding boundary conditions.

A general approach to the solution of this equation, applied to the study of traveling-wave tubes, was proposed in Ref. [24]. Later on, this approach was adopted in Refs. [7, 25] to the analysis of the space charge effects in the orotron. Following Ref. [25], we can write the final expression for $\overline{E}_{qy}$, which reads

$$\overline{E}_{qy}=\mathrm{Re}\left\{\frac{I_0}{i\omega\overline{S}\varepsilon_0}\sum_{n=1}^{\infty}\frac{1}{n}\left[i_n(y)\Gamma_{n0}+\sum_{m=1}^{\infty}(-1)^m \times\frac{\Gamma_{nm}}{n^m\beta_e^m}\frac{d^m i_n}{dy^m}\right]\times\exp[-in(\varphi_0+\Theta)]\right\}. \tag{14}$$

Here $\overline{S}=1/\int_S\Lambda^2(x,z)dx\,dz$ is the effective area of the beam cross section, and $i_n=\pi^{-1}\int_0^{2\pi}\exp[in(\varphi_0+\theta)]d\varphi_0$ is the nth harmonic of the beam current normalized at I_0. The coefficients Γ_{nm} are defined by

$$\Gamma_{nm}=\delta_0^m-[(i\beta_e n)^m/m!]\int_{-\infty}^{\infty}\mu^m\exp(in\beta_e\mu)G_2(\mu)d\mu, \tag{15}$$

where $G_2(y,y')=-\varepsilon_0\overline{s}\int_{S'}\int_S(x,z)\Lambda(x',z')[(\partial^2G/\partial x^2)+(\partial^2G/\partial z^2)]dx\,dz\,dx'dz'$ is the averaged Green's function $G(x,y,z,x',y',z')$ of the Poisson equation, and δ_0^m is Kronecker's symbol. Note that a useful relation holds for the coefficients Γ_{nm}:

$$\Gamma_{nm}=\frac{\beta_e^m}{m!}\frac{d^m\Gamma_{n0}}{d\beta_e^m}. \tag{16}$$

The coefficients Γ_{nm}, with $m=0$, stand for the conventional space charge reduction factors. The coefficients Γ_{nm} with $m\neq0$ determine a nonlocal action of the space charge field. However, because of the just quasilocal action of the Coulomb force, as a first-order approximation, the nonlocal phenomena can be neglected. The calculation of the coefficients given by Eq. (15) usually creates no difficulties if both Green's function and the distribution of the electron density over the beam cross section are known. In the case of electrons skimming over a diffraction grating, the well-known Green's function of the infinite metallic plane serves as a good approximation to this problem. A homogeneous distribution of the electrons over the beam cross section can be also assumed without serious influence on the accuracy of the Γ_{nm}-calculation. On this basis, an analytical expression was derived for Γ_{nm}, and for a ribbonlike beam, the result reads

$$\Gamma_{n0}=1-3/(2a_n)+(2/a_n)\exp(-a_n)-\exp(-2a_n)/(2a_n), \tag{17}$$

where $\sigma_n=n\beta_e a$. a is the beam thickness, which is assumed to be small compared with the beam width b. This expression, along with Eq. (16), allows us to determine the coefficients Γ_{nm}.

E. Mathematical model

The set of equations (9), (12), and (14) describes self-consistently the time evolution of the resonator field as well as its stationary states. The analysis of these equations can significantly be simplified for the case when the relaxation time $t_{\rm rel}$ of the resonator field is much larger than the transient time t_l of the particles through the interaction space. Since $t_{\rm rel}\approx Q/\omega_r$ and $t_l\approx 2r_y/v_0$, this is equivalent to the inequality

$$Q\gg 2r_y\omega_r/v_0. \tag{18}$$

This condition usually holds for orotron generators and amplifiers studied so far experimentally. Therefore, further analysis will be based on this assumption.

If condition (18) is met, the time variation of amplitude F and phase γ can be neglected during time intervals of the order of t_l. Separating the processes with different time scales in such a manner, we rewrite Eqs. (9) for the amplitude F and phase γ as follows:

$$\frac{dF}{d\tau}=[-1+GS_1(F,\gamma)]F+A_s\cos\gamma,$$

$$\frac{d\gamma}{d\tau}=[\delta-GS_2(F,\gamma)]+\frac{A_s}{F}\sin\gamma, \tag{19}$$

where functions

$$\begin{Bmatrix} S_1(F,\gamma) \\ S_2(F,\gamma) \end{Bmatrix} = \frac{1}{4\pi F}\int_0^{\tilde{L}}\Psi_m(\xi)\int_0^{2\pi}\begin{Bmatrix}\cos\\ \sin\end{Bmatrix} \times(\Phi_s\xi+\theta+\varphi_0+\gamma)d\varphi_0 d\xi, \tag{20}$$

called the oscillatory characteristics, are introduced. These functions in integral form describe the influence of a beam on the resonator field dynamics. To determine $S_1(F,\gamma)$ and $S_2(F,\gamma)$, the motion equation (12) must be solved for the values of F and γ, and for $\varphi_0\in[0,2\pi]$. Let us rewrite the equation of motion by taking into account expression (14) for the space charge field, but without the terms describing the nonlocal action of this field:

$$\frac{\partial^2\theta}{\partial\xi^2}=\left(1+\frac{1}{\Phi_0}\frac{\partial\theta}{\partial\xi}\right)^3\left\{\frac{F\Phi_0}{4}\Psi_m(\xi)\cos(\Phi_s\xi+\theta+\varphi_0+\gamma)-\frac{p_b^2}{\pi}\sum_{n=1}^{\infty}\frac{\Gamma_{n0}}{n}\int_0^{2\pi}\sin n[\tilde{\varphi}_0-\varphi_0+\theta(\tilde{\varphi}_0,\xi)-\theta(\varphi_0,\xi)]d\tilde{\varphi}_0\right\}. \tag{21}$$

Here $p_b=\omega_p r_y/\nu_0$, where $\omega_p=[|e|J_0/(m\varepsilon_0\nu_0)]^{1/2}$ is the plasma frequency. For the sake of further convenience, let us list all other control parameters of the model: $G=2Qr_y^2I_0/(\omega_r N_r U_0)$ is the gain (nonlinearity) parameter (see the Appendix); $\Phi_0=\omega r_y/\nu_0$ is the transient angle or the dimensionless radius of the field spot on the grating; $\Phi_s=\omega r_y(1/\nu_0-1/\nu_{\rm ph})$ is the velocity mismatch parameter; Γ_{n0}, $(n=1,2,3,\ldots)$ are the space charge reduction factors; $\Psi_m(\xi)$ is the mode amplitude distribution in the direction of particle motion; $\delta=2Q(\omega_r-\omega)/\omega_r$ is the normalized frequency detuning between the natural frequency of an excited mode and the frequency of an external signal; and A_s is the normalized amplitude of an external signal. It is obvious, that these parameters must be specified for each resonator in the case of a multiresonator amplifier.

The self-consistent set of equations (19)–(21), depending upon specific values of the control parameters, describes various modes of device operation, including amplification regimes, self-running oscillations, synchronization of oscillations, etc. It is worth noting that this model is also applicable to other types of resonance devices like the resonance backward-wave oscillator and the klystron with distributed interaction. Because of this, the natural question arises: Where do the peculiarities of the orotron manifest themselves? From the physical point of view, the main distinguishing feature of the orotron is the availability of a harmonic of the Smith-Purcell radiation, which produces the internal feedback and provides the energy output. This harmonic exerts almost no direct action on particle motion, and it is hence omitted in the motion equation. It nevertheless appears in the integral characteristic—the norm N_r, and therefore in the gain parameter G. The norm is proportional to the energy stored in the resonator, and its value is mainly defined by the harmonic of Smith-Purcell radiation. In this way, it produces an essential influence on the electron-wave interaction. This fact gives a general enough criterion for optimization of the orotron oscillatory systems by means of a minimization of the norm value (see the Appendix).

In addition, the Smith-Purcell harmonic, exciting an open resonator, forms the structure of the resonator field with some specific distribution. The slow wave, which interacts with the electron beam, becomes modulated according to this distribution, and it appears that the details of this distribution are also very important for the electron-wave interaction.

Solving Eqs. (19)–(21), one can directly find the time behavior of amplitude $F(\tau)$, phase $\gamma(\tau)$, and frequency $\omega_\mu(\tau)=\omega+(\omega_r/2Q)d\gamma/d\tau$ of an excited oscillation and/or the corresponding stationary values: $F_{\rm st}$, $\gamma_{\rm st}$, and $\omega_{\mu{\rm st}}$. Along with this, it is usually desired to calculate power characteristics like efficiency, power, and gain. The general expression for the power P_r stored by some resonator mode, is [22] $P_r=\omega_r N_r C_{\rm st}^2/(2Q)$, where $C_{\rm st}$ means dimensional steady-state amplitude of the field (1). In terms of the dimensionless amplitude F and the parameter G, this expression can be written as

$$P_r=P_0F_{\rm st}^2/G, \tag{22}$$

where $P_0=I_0U_0$ is the beam power. From this, we have an expression for the electron efficiency:

$$\eta=F_{\rm st}^2/G. \tag{23}$$

The dimensionless amplitude of the input signal A_s is determined by the power of the input signal $P_{\rm in}$, to be amplified in the following way:

$$A_s^2=(GP_{\rm in}/P_0)(1-|\Gamma|^2), \tag{24}$$

where Γ is the reflection coefficient at the resonator input terminal. This expression allows us to find the amplifier gain if the output power is known.

The set of equations (19)–(21) will be used in the next sections to study single-resonator orotron amplifiers. It should be noted that, in this case, a significant simplification of these equations can be achieved by virtue of the following fact. Since there is no preliminary beam modulation, the function $\Theta(\varphi_0,\xi)$ depends on the sum $\varphi\equiv\varphi_0+\gamma$ only rather than on φ_0 and γ separately. In this case, we have, instead of Eqs. (19),

$$\frac{dF}{d\tau}=[-1+GS_1(F)]F+A_s\cos\gamma,$$

$$\frac{d\gamma}{d\tau}=[\delta-GS_2(F)]+\frac{A_s}{F}\sin\gamma, \tag{25}$$

where the oscillatory characteristics depend on the field amplitude only:

$$\begin{Bmatrix} S_1(F) \\ S_2(F) \end{Bmatrix} = \frac{1}{4\pi F} \int_0^{\tilde{L}} \Psi_m(\xi) \int_0^{2\pi} \begin{Bmatrix} \cos \\ \sin \end{Bmatrix} \times [\Phi_s \xi + \theta(\varphi,\xi) + \varphi + \gamma] d\varphi_0 d\xi. \quad (26)$$

Thus the right side of these equation depends on γ in an explicit form, which obviously simplifies the problem of studying single-resonator amplifiers.

Another limiting case should be noted which corresponds to the self-running orotron. Setting $A_s = 0$, we find that the field dynamics is described by a single amplitude equation

$$\frac{dF}{d\tau} = [-1 + GS_1(F)]F, \quad (27)$$

whereas the second equation is transformed into a direct formula for the instantaneous frequency of oscillation $\omega_\mu(\tau) \equiv \omega + (\omega_r/2Q)(d\gamma/d\tau) = \omega_r[1 - (G/2Q)S_2(F)]$. Equations (26) and (27), or similar relations, have been intensively used to study single-mode operation of orotron oscillators [9–11,25].

III. A SINGLE-RESONATOR AMPLIFIER

To realize orotron amplification in the simplest way, one may use the conventional single-resonator orotron design just by transforming it into a reflection-type amplifier, as has schematically been shown in Fig. 1. Up to this day such an amplifier have mainly been studied experimentally [17,18]. Here we will analyze both the small- and large-signal operation modes of this amplifier for collective and single-electron interaction regimes.

A. Linear analysis

The single-resonator orotron amplifier shown in Fig. 1 is described by the system of equations (21), (25), and (26) with the initial conditions (13) for the equation of motion. This system is amenable to analytical treatment for the case of a linear mode of amplification. To find this solution, we start from the motion equation (21). To first order in amplitude F, its solution reads

$$\theta(\varphi,\xi) = (\Phi_0 F/4p) \int_0^{\xi} \Psi_m(\xi') \sin[p(\xi - \xi')] \times \cos(\varphi + \Phi_s \xi') d\xi',$$

which, after substitution into Eqs. (25) and (26) and some algebraic manipulations, yields the following equations for the resonator amplitude and phase:

$$\frac{dF}{d\tau} = \alpha_0 F + A_s \cos \gamma, \qquad \frac{d\gamma}{d\tau} = \delta_0 + \frac{A_s}{F} \sin \gamma, \quad (28)$$

Here $\alpha_0 = G\Phi_0 R_1(\Phi_s,p) - 1$ is a dimensionless rate of amplitude damping ($\alpha_0 < 0$) or growing ($\alpha_0 > 0$), and $\delta_0 = 2Q(\omega_0 - \omega)/\omega_r$ is the frequency detuning, with $\omega_0 = \omega_r[1 + G\Phi_0 R_2(\Phi_s,p)]$ the resonance frequency of the ''hot'' resonator. The functions R_1 and R_2 in the general case read

$$\begin{Bmatrix} R_1 \\ R_2 \end{Bmatrix} = \frac{1}{32p} \int_0^{\tilde{L}} \Psi_m(\xi) \int_0^{\xi} \Psi_m(\xi') \left[\begin{Bmatrix} \cos \\ \sin \end{Bmatrix} (\Phi_s + p)(\xi - \xi') - \begin{Bmatrix} \cos \\ \sin \end{Bmatrix} (\Phi_s - p)(\xi - \xi') \right] d\xi' d\xi, \quad (29)$$

where $p = \sqrt{\Gamma_{10}} \omega_p r_y / \nu_0$ is the space charge parameter. These functions go back to the linear theory of the orotron oscillator [2,7,26]. The function $R_1(\Phi_s,p)$ is proportional to the power delivered (or absorbed) by the beam. It is pertinent to make some comments concerning general properties of this function. In terms of the spatial spectral intensity $S_m(k)$ [see Eq. (5)], expression (29) for $R_1(\Phi_s,p)$ can be written in an alternate form (see also Refs. [27, 28]):

$$R_1 = (\pi/32pr_y^2)(S_1^- - S_1^+). \quad (30)$$

Here $S_m^{\mp} = S_m(k)|_{k=k_p^{\mp}}$ are values of the intensity calculated for k equal to the propagation constant $k_p^{\mp} = (\omega \pm \omega_p')/\nu_0$ of the slow and fast space charge waves, respectively, where $\omega_p' = \sqrt{\Gamma_{10}} \omega_p$ is the reduced plasma frequency. It is evident from Eq. (30) that the slow wave always gives up its energy to the resonator field, whereas the fast wave always absorbs the resonator energy.

Two limits of expression (30) are worth discussing in more detail. The first one is the single-particle interaction regime, which is defined by $2\omega_p'/\nu_0 \ll \Delta k$ (Δk is an characteristic width of the spatial spectrum of a synchronous wave), so that, from Eq. (30), we obtain

$$R_1 = \frac{\pi}{16 r_y^3} \left. \frac{dS_m(k)}{dk} \right|_{k=\beta_e}. \quad (31)$$

Here the derivative is evaluated for k, equal to the wave number $\beta_e \equiv \omega/\nu_0$ of a wave on the beam. Amplification of oscillations may occur only if $dS_m(k)/dk|_{k=\beta_e} > 0$, which physically means that in the vicinity of $k = \beta_e$, the spatial harmonics with a phase velocity (ω/k) less than ν_0 have larger amplitudes compared to those with $\omega/k > \nu_0$. For $m = 0$, the optimal value of Φ_s, maximizing the function $R_1(\Phi_s,0)$ and the amplifier gain as well, reads

$$\Phi_{s\ \mathrm{opt}} = -1. \quad (32)$$

Note that the inequality $dS_m(k)/dk|_{k=\beta_e} > 0$ may be considered as a generalized Cerenkov radiation condition, or it may be treated as the inverse Landau damping [29]. This condition enables one to determine, just from the form of the function $S_m(k)$, a range of varying β_e, where amplification may occur. It follows, e.g., from Eq. (5) that, for $m = 0$, β_e values must fall within the interval $k_1 - \Delta k/2 < \beta_e < k_1$ [$\Delta k \approx 1/r_y$ is the characteristic width of the spatial spectrum $S_m(k)$] in order that amplification occurs. For $m > 0$ the operation zone with respect to β_e (accelerating voltage) is split into $m+1$ subzones, since in this case the function $S_m(k)$ has $m+1$ maxima.

The second limiting case corresponds to the collective-electron (Raman) interaction regime with $2\omega_p'/\nu_0 \gg \Delta k$ when

$$R_1=[\pi/(32pr_y^2)]S_1^-, \tag{33}$$

provided that the value of $(\omega+\omega_p')/\nu_0$ is close to that of k_1. The optimal value of Φ_s, for this interaction regime, reads

$$\Phi_{s\ \mathrm{opt}}=-p. \tag{34}$$

The range of the β_e variation for $m=0$ [see Eq. (5)] is determined here by the condition

$$k_1-\Delta k/2<\beta_e+\omega_p'/\nu_0<k_1+\Delta k/2.$$

This range can be approximately two times larger than in the previous case.

Now we return to Eqs. (28). They can be solved analytically for the general case; however, we write only an expression for the amplitude of the steady-state oscillations, which is

$$F_{st}=A_s/(\alpha_0^2+\delta_0^2)^{1/2}. \tag{35}$$

The stable amplification regime can be realized only if $\alpha_0 \equiv G\Phi_0 R_1(\Phi_s,p)-1<0$; otherwise a self-excitation of the oscillations occurs in the device. The threshold (starting) value of the parameter G for self-excitation of the oscillations is given by

$$G_{th}=\frac{1}{\Phi_0 R_1(\Phi_s,p)}\equiv\frac{32pr_y^2}{\pi\Phi_0(S_1^- - S_1^+)}. \tag{36}$$

Let us now consider the amplification properties of the single-resonator orotron amplifier. Since this device is a reflection-type amplifier, we can use the following general expressions for the maximum midband gain [30]:

$$K=Q_h^2(2Q_{\mathrm{ext}}^{-1}-Q_h^{-1})^2, \tag{37}$$

and, for the half-power bandwidth,

$$\Delta\omega=\omega_0/Q_h. \tag{38}$$

Here Q_{ext} is the external Q of the resonator, and Q_h is the Q factor of the ''hot'' resonator, which includes all losses and their compensation due to an active medium in the resonator. It is easy to show, using Eqs. (28), that in our case Q_h is given by the following expression:

$$Q_h=Q_r/[1-G\Phi_0 R_1(\Phi_s,p)]. \tag{39}$$

For the resonator without beam we have $Q_h=Q_r$, where $Q_r^{-1}=Q_{\mathrm{ext}}^{-1}+Q_0^{-1}$ is the loaded Q factor, with Q_0 being the unloaded resonator Q. Now, taking into account Eq. (36), we can rewrite Eqs. (37) and (38) in terms of the orotron amplifier control parameters

$$K=(\Gamma+J)^2/(1-J)^2, \tag{40}$$

$$\Delta\omega=\omega_0(1-J)/Q_r, \tag{41}$$

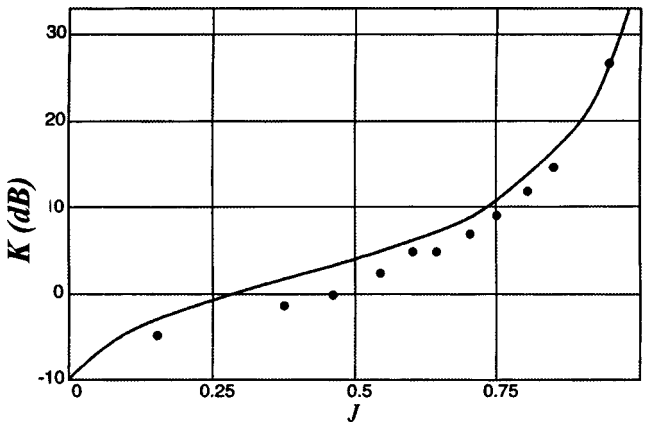

FIG. 3. Power gain vs normalized beam current for single resonator amplifier. Solid line—theoretical results; circles—experimental data [17,18].

where $J=G/G_{\mathrm{th}}$, and $\Gamma=1-2Q_r/Q_0$ is the reflection coefficient at the resonator input terminal. This form of presentation conveniently illustrates a typical feature for any reflection-type amplifier: an increasing gain and simultaneously decreasing bandwidth while approaching the threshold for self-excitation of oscillations. It should be noted that in the single-particle interaction regime ($p=0$), the function $R_1(\Phi_s,p)$ does not depend upon the beam current value. In this case and for a particular orotron amplifier, $J=I_0/I_{0\,\mathrm{th}}$ ($I_{0\,\mathrm{th}}$ is the threshold value of the beam current) if the beam current I_0 is considered as a variable parameter. This allows us easily to compare the analytical dependencies of $K(J)$ and $\Delta\omega(J)$ with corresponding experimental results. An example of such a comparison is given in Fig. 3, where the relationship between the amplifier gain and J, as given by Eq. (40), is displayed along with results of experimental investigations of 8-mm wave band amplifier with $U_0=2.5$ kV, $I_{0\,\mathrm{th}}=32.5$ mA, and $\Gamma=0.35$, which were described in Ref. [17]. Practically the same experimental data were obtained in recent experiments [18], with another design of the single-resonator orotron amplifier. Thus we can conclude that expression (40) fits the experimental data fairly well. In the latter case, the amplifier offers relatively high gain; the increase in the gain is, however, accompanied by a decreasing amplifier bandwidth according to Eq. (41). In this parameter region, nonlinearities of the electron-wave interaction may, however, have a pronounced effect on amplifier operation, so that they should be taken into account.

B. Effect of nonlinearities on small-signal amplifier operation

To study effects of nonlinearities on the small-signal amplifier operation, we take into account the first nonlinear terms in the F-power expansion of functions $S_1(F)$ and $S_2(F)$ [see Eq. (26)]. This gives the following equations for the amplitude and phase:

$$\frac{dF}{d\tau}=[\alpha_0-\alpha_1F^2]F+A_s\cos\gamma,$$
$$\frac{d\gamma}{d\tau}=[\delta_0-\delta_1F^2]+\frac{A_s}{F}\sin\gamma. \tag{42}$$

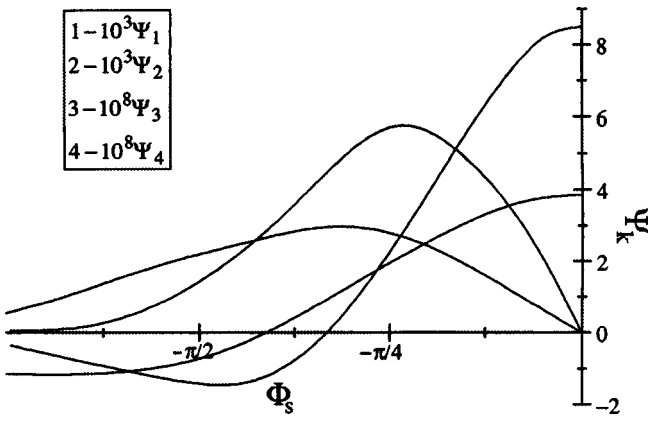

FIG. 4. Functions $R_i(\Phi_s,0)$, $i=1$, 2, 3, and 4.

Here $\alpha_1=\Phi_0^3 G R_3(\Phi_s,p)$ and $\delta_1=\Phi_0^3 G R_4(\Phi_s,p)$, where

$$R_{3,4}(\Phi_s,p)=(1/4)\int_0^{\tilde{L}}\Psi_m(\xi)(X_1^2+X_2^2)[X_{2,1}\cos(\Phi_s\xi) \mp X_{1,2}\sin(\Phi_s\xi)]d\xi,$$

$$\begin{pmatrix} X_1(\Phi_s,p) \\ X_2(\Phi_s,p)\end{pmatrix}=\frac{1}{8p}\int_0^{\xi}\Psi_m(\xi')\sin[p(\xi-\xi')] \times\begin{pmatrix}\cos(\Phi_s\xi') \\ \sin(\Phi_s\xi')\end{pmatrix}d\xi'.$$

The Φ_s dependence of functions R_3 and R_4, along with R_1 and R_2, is shown in Fig. 4 for the single-electron interaction regime ($p=0$) and a resonator mode with $m=0$. It should be noted that the function R_3 is positive at $\Phi_s<0$, i.e., in the amplification region where $R_1>0$. Hence the nonlinear term in Eq. (42) with R_3 describes the effect of a dissipative nonlinearity, whereas the second nonlinear term (with R_4) describes the effect of a reactive nonlinearity.

Setting $dF/d\tau=d\gamma/d\tau=0$ in Eq. (42), we find an equation for the amplitude F_{st}:

$$[(\alpha_0-\alpha_1 F_{st}^2)^2+(\delta_0-\delta_1 F_{st}^2)^2]F_{st}^2=A_s^2. \tag{43}$$

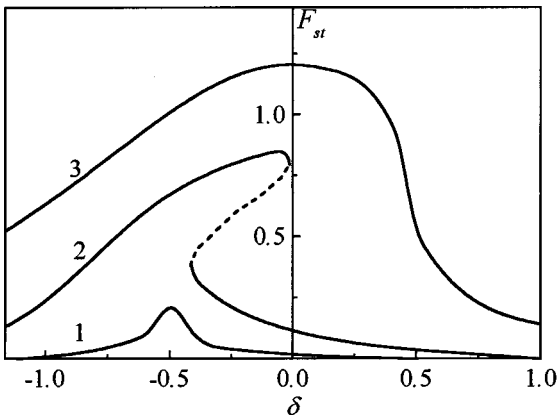

FIG. 5. Amplitude F_{st} of steady-state oscillations vs frequency detuning δ for different values of the normalized input power: (1) $P_{in}/P_0=-32$ dB, (2) $P_{in}/P_0=-28$ dB, and (3) $P_{in}/P_0=-12$ dB for $J=0.6$, and $\Phi_s=-0.65\pi$, $\Phi_0=25$, $p=0$, and $\Gamma=0$.

This is a cubic equation with respect to F_{st}^2. Hence the amplifier can have one or three stationary states. The latter case is realized for some region of the δ_0 variation only if the following conditions are simultaneously met:

$$A_s>A_{cr}\equiv\left[\frac{8|\alpha_0|^3(\delta_1^2+\alpha_1^2)}{3\sqrt{3}(|\delta_1|-\sqrt{3}\alpha_1)^3}\right]^{1/2}, \tag{44}$$

$$|\delta_1|>\sqrt{3}\alpha_1. \tag{45}$$

Thus, for multistationary states to arise the signal amplitude A_s should be in excess of the value A_{cr} given by Eq. (44). In addition, the parameter of the reactive nonlinearity should be larger than some limit, which is determined by the dissipative nonlinearity given in Eq. (45). When conditions (44) and (45) are met, the δ dependence of the steady-state amplitude F_{st} (resonance curve of the amplifier) is characterized by the existence of a hysteretic loop, which is illustrated by curve 2 in Fig. 5. The resonance curves in this figure have been found from the solution of the initial system (25), and there behavior is sufficiently well described by the approximate model of Eq. (42) provided that A_s is not too large. At large values of A_s, higher nonlinear terms, which are not included in Eqs. (42), manifest themselves. This leads, for example, to the effect of suppressing the bistability, which is illustrated by curve 3 in Fig. 5. This effect is not described by Eqs. (42).

It is easy to show, by using the standard stability analysis of equilibria, that in the hysteretic region the states with the largest and smallest values of the amplitude are always stable, whereas the third state is always unstable. Hence, in this case, the amplifier is altered to a bistable device, and the one-to-one correspondence between the amplifier input and output is violated. This can be considered as a specific form of amplifier instability (see Sec. III C).

Let us now consider the case when the amplitude A_s is below the critical level, so that the one-to-one correspondence is preserved. Here Eq. (43) can be solved by using a successive approximation procedure and by considering the terms $\alpha_1 F_{st}^2$ and $\delta_1 F_{st}^2$ as a perturbation. Choosing the value of F_{st} from Eq. (35) as first approximation, the second approximation reads

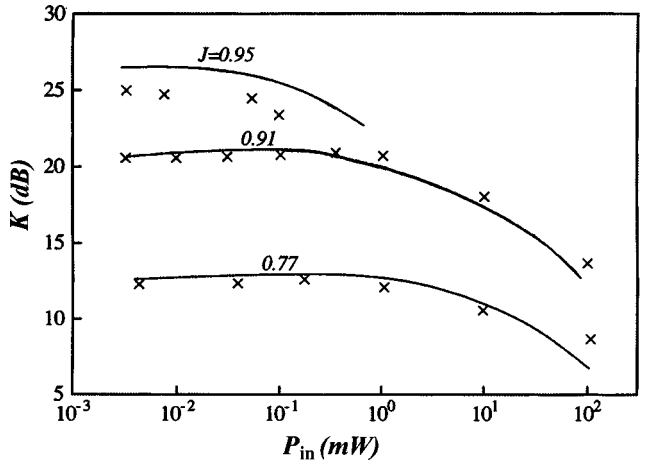

FIG. 6. Power gain vs P_{in} according to Eq. (47) (solid lines) and experimental data (crosses) for different values of J at $\Phi_s=-1$, $\Gamma=0.35$, $U_0=2.5$ kV, $I_{0\,th}=32.5$ mA, and $\Phi_0=100$.

$$F_{\rm st}^2=A_s^2\left[\left(\alpha_0-\frac{\alpha_1 A_s^2}{\alpha_0^2+\delta_0^2}\right)^2+\left(\delta_0-\frac{\delta_1 A_s^2}{\alpha_0^2+\delta_0^2}\right)^2\right]^{-1}. \quad (46)$$

As one can expect, the amplitude of the forced oscillations has always a finite value because of the nonlinearities (recall that $\alpha_0<0$ and $\alpha_1>0$), and the central frequency of the amplifier becomes dependent on the amplitude of the input signal. To find an expression for the amplifier gain, we again make use of Eq. (37). The Q factor of the ''hot'' resonator Q_h can in this case be found from Eq. (42). The result reads

$$Q_h=\frac{Q_r}{-\alpha_0+\alpha_1 F^2}\equiv\frac{Q_r}{1-G\Phi_0 R_1(\Phi_s,p)+G\Phi_0^3 R_3(\Phi_s,p)F^2}.$$

After the substitution of this expression into Eq. (37), and some transformations, we arrive at the following formula for the gain:

$$K=\frac{(\Gamma+J)^2}{\{1-J+J^2(1-J)^{-2}\Phi_0(1-|\Gamma|^2)(P_{\rm in}/P_0)[R_3(\Phi_s,p)/R_1^2(\Phi_s,p)]\}^2}. \quad (47)$$

The relationship between the input power ($P_{\rm in}$), the beam power (P_0), and the amplitude A_s is given by Eq. (24). The dependence of K on $P_{\rm in}$, as given by Eq. (47), is shown in Fig. 6 for the single-electron-interaction regime at $\Phi_s=-1$, $\Gamma=0.35$, and $\Phi_0=100$. This Φ_s value is optimum for the linear case, and the chosen Φ_0 and Γ values are approximately the same as in the above mentioned experiments [17]. The corresponding experimental results given in Fig. 6 are in good agreement with the theoretical curves. As can be seen from this figure, the effect of the input power is increased when the J value approaches unity, i.e., when the beam current approaches the threshold value $I_{0\,\rm th}$. The increase in the input power leads to a gain lowering effect, as can be seen from Eq. (47) if we take into account that $R_3(\Phi_s,p)>0$ in the amplification regime. The dynamic range of the amplifier is dramatically reduced when the amplifier is operated near threshold of self-excitation ($J=1$). The increase of the transient angle Φ_0 also contributes to decreasing the dynamical range.

C. Stability analysis

From the point of view of the theory of dynamical systems, instabilities in an amplifier are due to bifurcations occurring in the system. In the framework of the mathematical model (25), three types of bifurcations may be responsible for instabilities, namely supercritical and subcritical Hopf bifurcations, and the saddle-node bifurcation. Rigorous mathematical definitions of these bifurcations can be found, e.g., in Ref. [31]. We will deal here with their impact on the dynamics and stability of the amplifier.

Let us start from the supercritical Hopf bifurcation, which leads to a soft self-excitation of oscillations. The term *soft* stands for the fact that the state with $F=0$ becomes unstable, and an arbitrary small perturbation initiates the orotron oscillation generation. According to the stability analysis of system (28) or (42), this occurs when the α_0 value becomes positive. This gives the following stability condition:

$$G<G_{\rm th}\equiv[\Phi_0 R_1(\Phi_s,p)]^{-1}. \quad (48)$$

It is convenient to analyze this condition on the parameter plane $(\Phi_0 G,\Phi_s)$, which is shown in Fig. 7 for the single-particle interaction regime $p=0$. The curve $\Phi_0 G_{\rm th}=[R_1(\Phi_s,0)]^{-1}$, separating stable and unstable regions of operation, is plotted here for the case $m=0$. Note that, for a practical amplifier, the variation of the parameter Φ_s may be related to an accelerating voltage variation, whereas the parameter G is proportional to the beam current value. The amplification ($K>1$) may occur only if $\Phi_s<0$. Expression (40) for the amplifier gain is valid for any Φ_s-value in this range, but to obtain a high K value with a minimum beam current, the parameter Φ_s must be chosen as $\Phi_s=\Phi_{s\,\rm opt}$, where $\Phi_{s\,\rm opt}$ is given by Eq. (32), and the corresponding minimum value of the parameter $G_{\rm th}$ is

$$G_{\rm th\,min}=17/\Phi_0. \quad (49)$$

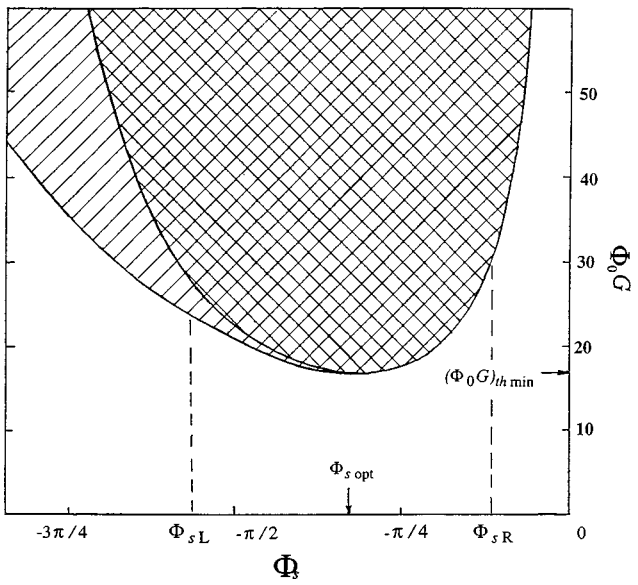

FIG. 7. Regions of stable and unstable amplifier operation in the parameter plane $(\Phi_0 G,\Phi_s)$. In the doubly and singly shaded regions, soft and hard types of self-excitation of oscillations occur, respectively. Vertically dashed lines denote the boundary of the saddle-node bifurcation onset. Region $\Phi_{sL}<\Phi_s<\Phi_{sR}$ is the safe region with respect to this bifurcation.

By using Eq. (A15) for the norm of a quasi-TEM_{20q} mode, we find the following expression for the minimum threshold value of the beam current:

$$I_{0\text{th min}} \cong 0.3\left(\frac{|e|}{m}\right)^{1/2} \frac{(q+1/2)r_x\Theta_d}{\omega_r r_y^2 W Q_r}\, U_0^{3/2}. \tag{50}$$

Here W is the wave resistance of the free space, and the coefficient $\Theta_d > 1$ takes the finite width of the grating grooves into account [see Eq. (A9)]. When deriving this expression, beam thickness a and beam width b have been chosen to be optimum (see the Appendix), and read

$$b = 0.8 r_x, \quad a = 1.2\nu_0/\omega_r. \tag{51}$$

In the following, these values are used for the analysis and the amplifier parameter estimates. Recall that the physical meaning of these values is as follows: They maximize the gain parameter G for a given value of the beam density.

In the collective-electron interaction regime, the parameter plane $(\Phi_0 G, \Phi_s)$ has in general the same structure as in the previous case. The threshold curve $\Phi_0 G_{\text{th}} = [R_1(\Phi_s, p)]^{-1}$ for $p \gg 1$ reads

$$\Phi_0 G_{\text{th}} = (64p/\pi)\exp[(\Phi_s - p)^2/2].$$

Thus a minimal value of G_{th}, equal to

$$G_{\text{th min}} = 64p/(\pi\Phi_0), \tag{52}$$

is obtained at $\Phi_{s\ \text{opt}} = -p$, which is equivalent to $k^- = k$. Making use of Eq. (A15) and of the definitions of the parameters p, Φ_0, and G, we rewrite Eq. (52) with respect to the minimum value of the threshold current for the case of a quasi-TEM_{20q} mode

$$I_{0\text{th min}} \cong 3\times 10^3 \frac{\varepsilon_0 c^2 \Gamma_{10}(q+1/2)^2 U_0 r_x \Theta_d^2}{\omega_r r_y^2 Q_r^2}. \tag{53}$$

As was mentioned before, in the region above the threshold curve in Fig. 7 (double-shaded region), a soft self-excitation of oscillations occurs in the orotron. However, the hard type of the orotron self-excitation may also be realized, and the subcritical Hopf bifurcation is responsible for this process. Unlike the previous case, the occurrence conditions cannot be found here analytically from a small-signal analysis. It can only be noted that, for $m = 0$, this type of excitation may be realized only if $\Phi_s < \Phi_{s\ \text{min}}$. Direct numerical studies are necessary to determine the location of regions in the parameter space where the hard excitation of oscillations takes place. The corresponding region is shown on the parameter plane in Fig. 7. In this region, the trivial state $(F = 0)$ of the autonomous system $(A_s = 0)$ is stable; a stable periodic orbit, however, also exists in the phase space of system (25). An external signal of finite value can trigger the system from the trivial state on the periodic orbit to cause the excitation of orotron oscillations. As can be seen from Fig. 7, the hard excitation of oscillations occurs at lower values of the parameter G as compared to the soft excitation. This leads to a decrease of the G values which may be used for the amplification regime.

Additional limitations for the choice of the parameter G as well as of other parameters result from the saddle-node bifurcation onset. This bifurcation manifests itself in the following way. If the amplitude of an external signal (A_s) passes through some critical value (A_{cr}), a stable state is split into three states: two stable states and an unstable (saddle) state. In terms of the amplifier resonance curve, this is exhibited by a hysteretic loop shown on Fig. 5. It should be stressed that each of these stable states corresponds to forced oscillations with the frequency of the external signal, and, opposite to the Hopf bifurcations, a self-excitation of oscillations does not occur. However, the simultaneous existence of two stable states with different values of the output amplitude is undesirable for most amplifier applications. Also, as follows from general results concerning the stability of quasiperiodically forced systems [32], in this case chaotic oscillations may easily arise when a real multiperiodic signal is applied at the amplifier input.

Approximate conditions for the occurrence of the saddle-node bifurcation are given by Eqs. (44) and (45). Note that Eq. (45) is equivalent to the following one:

$$|\Psi_4(\Phi_s, p)| > \sqrt{3}\Psi_3(\Phi_s, p). \tag{54}$$

Referring to Fig. 3, we find that for the single-electron interaction regime this condition is satisfied if Φ_s is outside the interval

$$-0.55\pi \equiv \Phi_{sL} < \Phi_s < \Phi_{sR} \equiv -0.1\pi. \tag{55}$$

The corresponding boundaries of the regions where the saddle-node bifurcation may arise are also indicated in Fig. 7. To avoid the onset of the saddle-node bifurcation and of the related instability, one should try to choose Φ_s (the accelerating voltage) within the ''safe region'' given by Eq. (55). It is easy to remove the threat of this instability for small-signal amplifier operation, since, for this case, the optimal value of $\Phi_s = -1$ is within that region. However, in the case of large-signal amplifier operation, optimal values of Φ_s are less than -1, and they may be located outside of the ''safe region.'' For this case, the instability may manifest itself even if J is relatively small, for instance, as in Fig. 5 (see curve 2). Curve 3 in this figure illustrates a possibility to suppress the instability of this type. As follows from the initial model (25), when the power of the input signal is large enough, the hysteretic loop on the resonance curve disappears. This phenomenon is a principally nonlinear one. Thus the discussed instability may appear if the amplitude of the input signal lies within an interval $A_{\text{cr}} < A_{\text{in}} < A_{\max}$, where A_{cr} is approximately determined from Eq. (44), and $A_{\max}$ can be found numerically.

The results of this section clearly indicate that values of the control parameters, which can be used for an amplifier design, are seriously limited by instabilities of various types. In particular, the self-excitation of oscillations and other instabilities are factors (but not the only ones) which limit essentially the maximum beam current value which can be used in a particular design. Referring to Fig. 6, we note that for Φ_s from the region $\Phi_s < \Phi_{s\ \text{opt}} \equiv -1$, an operating value of the current can be large then the minimum threshold current which is achieved at $\Phi_s = -1$. As is also seen from this figure, such an increase in the current cannot be too large due

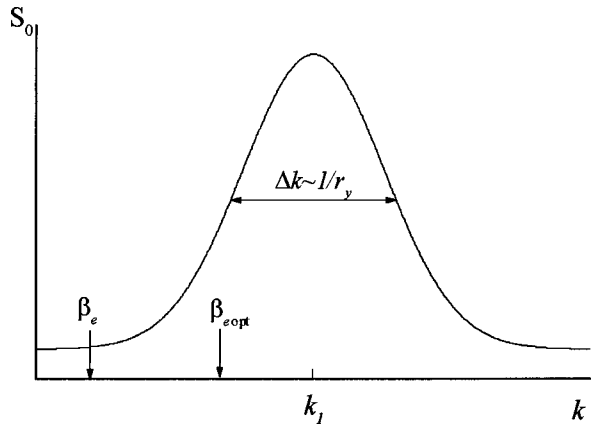

FIG. 8. Schematic of the spectrum-shape function $S_m(k)$ for $m=0$ with its maximum at $k=k_1$ and the location of the optimal value of the beam wave number in the linear interaction regime ($\beta_{e\ \mathrm{opt}}$) and in the nonlinear regime (β_e).

to the limitation on the minimum value of Φ_s imposed by the instabilities. Due to this we accept that $G_{\mathrm{th\ min}}$ and $I_{0\mathrm{th\ min}}$, given by Eqs. (49) and (50) for the single-electron interaction regime and by Eqs. (52) and (53) for the collective one, are the maximum possible values of the parameter G and the beam current for nonlinear regime of amplification.

D. Large-signal amplifier operation

Before going into detail about the large-signal amplification mode, it is appropriate to remember some general properties of electron-wave interaction in the orotron-type tubes. In the linear regime, the amplifier gain and output power are determined by local properties of the function $S_m(k)$, namely, by the value of its derivative calculated at $k=\beta_e$ [see Eq. (31)], because any variation of the electron velocity by the action of the field is small. In the nonlinear regime, the effect of the mean velocity decrease of the electrons is of principal importance. Introducing the *current propagation constant* $\beta_{e\ \mathrm{cur}}(\varphi,y)\equiv\omega/\nu(\varphi,y)$, we may treat this effect as a diffusion of the $\beta_{e\ \mathrm{cur}}(\varphi,y)$ values in the wave package toward a peak of the spectrum $S_m(k)$ (see Fig. 7). The maximum value of $\beta_{e\ \mathrm{cur}}(\varphi,y)$ is limited by the value of k_1, since at $\beta_{e\ \mathrm{cur}}>k_1$ the Cerenkov radiation condition is not fulfilled, and the electrons cannot be decelerated any more. The minimum possible value for β_e is determined by the capability of a wave spectral component with $k=\beta_e$ to trap into a potential well an essential portion of electrons from those entering the interaction space during the field time period. The process of trapping is a threshold phenomenon, and the amplitude of this spectral component must overcome a critical value [33]. From Fig. 8 it is clear, that because of this threshold, the maximum value of the difference $(k_1-\beta_e)$ for $m=0$ is of the order of $\Delta k\approx 1/r_y$, which is the bandwidth of the spectrum $S_0(k)$. Utilizing the estimates given above, one can obtain the following scaling low for the maximum efficiency in the nonlinear interaction regime

$$\eta_{\max}\approx\nu_0\lambda/(cr_y)\quad\text{or}\quad\eta_{\max}\approx 2\pi/\Phi_0. \tag{56}$$

Such a dependence of the maximum efficiency on the wavelength or on the transient angle $\Phi_0\equiv 2\pi(r_y/\lambda)(c/\nu_0)$ has been reported with respect to various kinds of free-electron lasers and conventional microwave tubes [8,9,34].

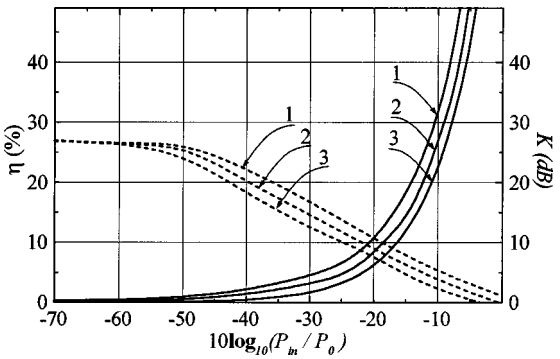

FIG. 9. Maximum electron efficiency (solid curves) and maximum gain (dashed curves) vs P_{in}/P_0 for various values of the transient angle: (1) $\Phi_0=25$, (2) $\Phi_0=50$, and (3) $\Phi_0=100$ at $J_0=0.95$, $p=0$, and $\Gamma=0$.

Let us now consider the effect of the Φ_0 value on the orotron amplifier performance. In Fig. 9, maximum efficiency and gain are shown versus P_{in}/P_0 for various values of Φ_0. The ''maximum'' hereinafter means that the parameters Φ_s (the accelerating voltage) and δ (frequency of the input signal) have been chosen to be optimum for each particular set of parameters. It can be seen from Fig. 9 that when the input power is relatively small, the efficiency and gain do not practically depend on Φ_0, as predicted by the linear theory. This dependence, which is pronounced at a large level of the input signal, leads to an increase in efficiency and gain with decreasing Φ_0, in accordance with the arguments given above. It should be noted, however, that the variation of η and K with the Φ_0 variation is essentially slow compared to that of $1/\Phi_0$, even if $P_{\mathrm{in}}\approx P_0$. The reason for this is related to the fact that it is impossible to trap most of the electrons entering the resonator into a potential well during a time period if the same interaction space is used for both the beam modulation by an external signal and the deceleration of the electrons by the resonator field. The latter also does not allow one to reach high values of gain and efficiency simultaneously (see Fig. 9), because the optimum set of parameters for effective modulation and bunching is in general quite different from that for effectively decelerating the electrons. To obtain high values for the efficiency (40% and higher), large levels of the input signal are necessary, which naturally leads to a decrease of the gain. It is obvious that, to get rid of this problem, a preliminary modulation of the beam must be used, like in conventional klystrons or klystrons with distributed interactions. Our analysis has shown that a dramatic improvement of amplifier performance can be obtained even by using the two-stage amplifier design shown in Fig. 2 (corresponding results will be published).

However, it should be pointed out that the single-resonator orotron amplifier may also be of practical interest when taking into account the simplicity of its design. Hence we will give some more details to describe its performance. An expression for the maximum output power in the single-electron interaction regime may be written in the form

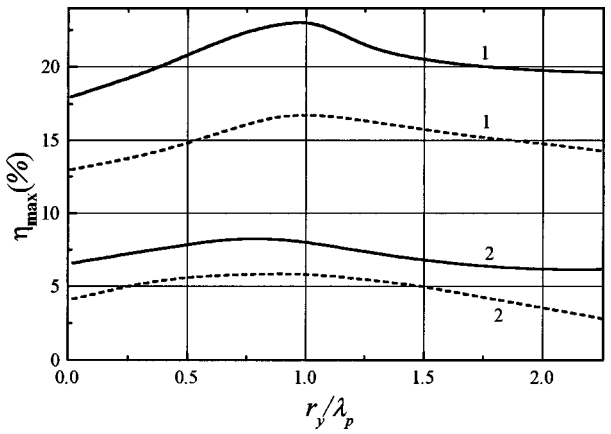

FIG. 10. Maximum electron efficiency vs $r_y/\lambda_p \equiv p/2\pi$ for $\Phi_0 = 25$ (solid curves) and $\Phi_0 = 50$ (dashed curves) for different values of the input power: (1) $P_{in}/P_0 = -15$ dB and (2) $P_{in}/P_0 = -25$ dB at $J_0 = 0.95$, $\sigma_1 = 1.2$, and $\Gamma = 0$.

$$P_{\text{out max}} \cong 14\varepsilon_0 \left(\frac{|e|}{m}\right)^{1/2} \frac{(q+1/2)\lambda r_x \Theta_d}{r_y^2 Q} \times U_0^{5/2} \eta_{\max}(\Phi_0, P_{\text{in}}/P_0), \tag{57}$$

provided that the beam current value is equal to the maximum possible value given by Eq. (50), and the dimensions of the beam cross section are optimal: $a = 1.2\nu_0/\omega$ and $b = 0.8 r_x$. The maximum efficiency is a function of Φ_0 and the normalized input power as illustrated in Fig. 9. To illustrate typical values of the parameters involved here, let us consider an amplifier at $\lambda = 3$ mm with 16-kV electron beam voltage and a resonator with $r_y = r_x = 3$ mm, $Q = 1000$, and the TEM_{203} operating mode. In this case, the beam current value may be as high as 380 mA, with a density of 110 A/cm^2. Such a device could provide a gain of 14 dB with an efficiency of 7% and an output power of 400 W, or a gain of 8 dB with an efficiency of 18% and an output power over 1 kW depending on the level of the input signal. With the same beam voltage, current density, and resonator parameters, a reduction of the operating wavelength by four times, i.e., to 0.75 mm, will lead to a lowering of the efficiency by a factor of 2 and of the output power by a factor of 8. According to Fig. 9 and Eq. (57), in order to reduce the effect of the wavelength on the amplifier performance, one should try to decrease the radius r_y, correspondingly increasing the beam density. In this case, it necessary to take into account that the limiting value of the beam density may not only be determined by rising self-running oscillations, but also by other factors like emitting capabilities of a cathode and space-charge effects.

If the density is limited by the emission capabilities of a cathode, we then have

$$P_{\text{out max}} \cong (0.2/c)\sqrt{|e|/m} J_0 r_x \lambda U_0^{3/2} \eta_{\max}(\Phi_0, P_{\text{in}}/P_0).$$

Here the output power depends on the accelerating voltage as to a smaller degree than in the previous case, but the dependence on the wavelength remains the same.

To illustrate the space charge effect on the amplifier performance, we start from Fig. 10, where the maximum efficiency is plotted as a function of the ratio $r_y/\lambda_p \equiv p/2\pi$ [$\lambda_p \equiv 2\pi\nu_0/(\sqrt{\Gamma_{10}}\omega_p)$ is the beam plasma wavelength]. It is seen from this figure that the efficiency peaks at some value of the parameter p (plasma frequency). The physical reasons for this are the following. In the collective electron interaction regime, the electrons are trapped by the spectral components from the ''left tail'' of the spatial spectrum (see Fig. 8). Then electrons can transfer some amount of their energy to the resonator field due to the decrease of their mean velocity, like in the single-electron interaction regime. There is, however, an essential difference between these two cases, which lies in the fact that in the Raman regime, the interaction of the slow space charge wave with any of the spatial spectral components of the field leads to an energy extraction from the beam [see Eq. (33)], i.e., not only with those where $dS_m(k)/dk > 0$ at $k = \beta_e$ as in the single-electron interaction regime. Due to that the decrease of the velocity of electrons during their interaction with the field can be larger, which can result in a rise of the efficiency. However, the space charge field can also affect electron-wave interaction in an opposite way, which may be approximately described as the retarding of the formation of compact electron clusters needed for an effective deceleration of the electrons. Both effects—upgrading and degrading of the amplifier performance due to the space charge field—are seen in Fig. 10. However, the increase of the efficiency is not too large compared to the single-electron interaction regime.

The presented results give also evidence that in a wide range of the plasma frequency (beam density) variation, the space charge effects do not impose serious limitations on the efficiency. For example, for the above considered 3-mm wave amplifier with a beam density of 110 A/cm^2 and a ratio $r_y/\lambda_p = 0.05$, the space charge effects are practically negligible. It should be noted that for the case of relatively large p values (practically it corresponds to $p \geqslant \pi$), the maximum possible value of the beam current which can be used in the collective regime is given by Eq. (53).

IV. DISCUSSION AND CONCLUSIONS

In this paper, a mathematical model of orotron-type amplifiers has been presented, which is general enough to describe various amplification regimes in single-stage and multistage amplifiers as well as self-running oscillations, synchronization of oscillations, and frequency conversion depending on the choice of the control parameters. In the linear mode of amplification, the model equations are solved analytically for both collective and single-electron interaction regimes when studying the single-resonator amplifier. Effects of nonlinearities on the small-signal operation mode have also been studied analytically. These theoretical results have been compared with experimental data obtained so far for single-resonator amplifiers, and both qualitative and quantitative correspondences have been found.

Simulations of the large-signal nonlinear amplification mode have been preceded by a detailed stability analysis of the amplifier. Soft and hard excitations of self-running oscillations along with arising bistable states are three main types of instability of the amplifier. The first two of them impose limitations on the maximum value of the gain parameter (beam current value), which can be used in the amplifier. The third one is related to anharmonic properties of the reso-

nator loaded by the beam. The bistability may occur in some regions of the amplifier operation zone with respect to the accelerating voltage, even if the parameter G is essentially lower than its threshold value.

It should be emphasized, however, that in practical amplifiers additional instabilities may arise due to the interaction of resonator modes. So far this interaction has been only studied with respect to the stability of orotron oscillators (see, e.g., Refs. [13,14]). The corresponding analysis with respect to orotron amplifiers is an unsettled problem.

The investigation of the large-signal amplification mode has shown that, in the single-resonator amplifier design, it is impossible to simultaneously obtain the maximum possible values of the efficiency and large values of the gain. This is because the effective bunching of the beam and the deceleration of the electrons cannot be arranged within a single interaction space beam, and the deceleration of the electrons cannot be arranged within a single interaction space. The natural solution of the problem lies in the application of at least a two-stage amplifier in order to separate these processes. However, even a single-resonator amplifier is of practical interest, especially taking into account the simplicity of its design and fabrication, the ease of cooling, and the possibility to operate it in the millimeter- and submillimeter-wave bands, and probably even above. For example, a 3-mm wave amplifier can provide a gain of 14 dB with an efficiency of 7% with a 16-kV beam. The efficiency and the output power of the amplifier grow up with a decrease of the radius of the field spot, which means an effective length of the interaction space. Such a dependence on the length of the interaction space is typical of various types of Cerenkov-type devices. In this respect, the orotron shows an obvious advantage over classical devices like the klystron with distributed interaction, where the interaction length coincides with the geometrical length. In the orotron, the length of the interaction space—the radius of the field spot—is controlled by the curvature of the upper mirror and by mirror separation, and, due to it the geometrical length of the grating and the dimensions of the mirrors, can be essentially larger. This provides a possibility to choose these dimensions according to other demands, for example, related with cooling or providing a desired value of the Q factor.

It should be noted that with decreasing the radius of the field spot, the beam density should be increased to provide a high level of the amplifier performance. In this connection, an important result is that the space charge field effects practically do not impose limitations on the maximum value of the beam current which may be used in the orotron amplifier. This opens an additional possibility to operate the orotron amplifiers at rather short wavelengths.

ACKNOWLEDGMENTS

This work was supported in part by EC under Contract No. ERBIC15CT960816. D.V. acknowledges support from the Technical University Hamburg–Harburg.

APPENDIX: NORM CALCULATION

We give an example of the norm calculation for an arbitrary quasi-TEM$_{smq}$ mode of a semispherical open resonator with a grating similar to that widely used in orotron oscillator design [1,2,4] (see also Fig. 1). In the general case, the norm is defined as

$$N_r=\varepsilon_0\int_V \vec{E}_r\cdot\vec{E}_r^{*}dV. \tag{A1}$$

The expression for the E_{ry} component of the field is given by Eq. (2). The other nontrivial field components, which are H_{rx} and E_{rz}, can be easily found from Maxwell's equations.

When performing the integration in Eq. (A1), it is possible to neglect the direct contribution from the slow waves. This is apparent from the fact that these waves occupy a small volume compared to the harmonic of the Smith-Purcell radiation, and because their amplitudes are smaller than that for slow-wave harmonics (see below). As a result, we have

$$N_r\cong\varepsilon_0 A_0^2\int_V \Psi_s^2(x)\Psi_m^2(y)\cos^2 k_r(z-D)dV. \tag{A2}$$

Using expression (7) for the normalized coefficient A_0, we transform Eq. (A2) to a form

$$N_r=\frac{a_0^2\varepsilon_0\int_V \Psi_s^2(x)\Psi_m^2(y)\cos^2 k_r(z-D)dV}{4a_1^2\left[\int_S \Lambda(x,z)\Psi_s(x)\exp(-|\gamma_1|z)dx\,dy\right]^2}. \tag{A3}$$

The integration in the numerator is performed over the whole volume of the resonator, and that in the denominator is performed over the cross section of the beam. The ratio of the harmonic amplitudes a_n/a_0 can approximately be determined by using the model of an infinite (in x and y directions) grating. This model yields [26]

$$\frac{a_n}{a_0}=\frac{\sin(k_r h)\sin(\pi n d/l)}{\pi n\sqrt{\cos^2(k_r h)+(d/l)^2\sin^2(k_r h)}}, \tag{A4}$$

where l is the grating period, and d and h are, respectively, the width and depth of the grating grooves.

The efficiency of both the orotron oscillator and amplifier rises with an increase of the parameter G. Since $G\propto 1/N_r$, such an oscillatory system is optimum for the orotron in which N_r reaches a minimum value. The physical reason for this stems from the fact that the norm inversely depends on the intensity of the slow wave interacting with the beam [see Eq. (A3)].

It follows from Eqs. (A3) and (A4) that the optimal values of the groove depth are

$$h=\lambda/4+\lambda n/2 \quad (n=0,1,2,\ldots), \tag{A5}$$

when the ratio a_1/a_0 becomes

$$a_1/a_0=\sin(\pi d/l)/(\pi d/l). \tag{A6}$$

Let us now specify the model for the electron beam. We assume that the whole beam, having a homogeneous density distribution, is concentrated in a cross section S of rectangular form, which is described as

$$0<z<a, \quad -b/2<x<b/2$$

with a and b the thickness and width of the beam, respectively. In this case, the function $\Lambda(x,z)$ reads, in accordance with the normalization condition (8),

$$\Lambda(x,z)=\begin{cases}1/(ab) & \text{at } x,z\in S\\ 0 & \text{elsewhere,}\end{cases} \tag{A7}$$

Substituting Eqs. (A6) and (A7) into Eq. (A3), we arrive, after some transformations, at the expression

$$N_r=\frac{\varepsilon_0 b r_y D}{8}\left(\frac{1}{\sin^2(k_r D)}+\frac{\operatorname{cotan}(k_r D)}{k_r D}\right)\chi_x\chi_y\chi_z\Theta_d. \tag{A8}$$

Here

$$\chi_x=u\int_{-\infty}^{\infty}\Psi_s^2(\tilde{x})d\tilde{x}\left[\int_{-u/2}^{u/2}\Psi_s(\tilde{x})d\tilde{x}\right]^{-2},$$

$$\chi_y=\int_{-\infty}^{\infty}\Psi_m^2(\xi)d\xi,$$

$$\chi_z=\frac{\sigma_1^2}{[1-\exp(-\sigma_1)]^2},\quad \Theta_d=\left[\frac{\pi d/l}{\sin(\pi d/l)}\right]^2, \tag{A9}$$

where $u=b/(2r_x)$, $\tilde{x}=x/(2r_x)$, and $\sigma_1=2\pi a/l (l\ll\lambda)$, $\xi=y/r_y$. Note that the integrations in Eq. (A9) are performed in infinite limits rather than in finite ones. Such a substitution of the limits is possible because of the exponential decay of the resonator field to zero when approaching the resonator boundary.

For a resonator with a grating partially covering the bottom mirror in the x direction, the mode with $m=0$ and $s=2$ is the principal one, and for this case the coefficients χ_x and χ_y become

$$\chi_x=2u\sqrt{2/\pi}[\operatorname{erf}(u)-(4u/\sqrt{\pi})\exp(-u^2)]^{-2},\quad \chi_y=\sqrt{\pi/2}, \tag{A10}$$

where $\operatorname{erf}(u)=(2/\sqrt{\pi})\int_0^u \exp(-t^2)dt$.

Considering χ_x as a function of the normalized beam thickness u, we find that this function possesses two minima at $u=0.4$ and 2, and consequently there are two values of the beam width, which may be used in practice: $b=0.8r_x$ and $b=4r_x$. The b value of $b=0.8r_x$ is actually chosen in practical devices [2], so that it is used in our estimates.

From Eq. (A4), it follows that the norm depends on the distance between the mirrors D in a resonant way. The minimum is attained at $D=q\lambda/2+\lambda/4$, where $q=1,2,3,\ldots$ is the number of half-waves kept between the mirrors. Provided that the resonator and beam parameters are chosen to be optimum, as indicated above, the norm of the quasi-TEM_{20q} mode becomes equal to

$$N_r=0.4\varepsilon_0\lambda(q+1/2)r_x r_y\chi_z\Theta_d. \tag{A11}$$

The coefficients Θ_d and χ_z take the finite width of the grating grooves and of the beam thickness into account, respectively. With the norm value given by Eq. (A11), the parameter G reads

$$G\cong\frac{0.8WQr_y I_0}{r_x(q+1/2)\chi_z\Theta_d U_0}. \tag{A12}$$

Note that usually $r_x=r_y$, and thus the G value does not directly depend on the dimensions of the field spot for some chosen value of the beam current value. In many cases, however, the beam density J_0 is a limiting factor, and we should put I_0 into Eq. (A12) as $7=abJ_0$. Now it can be seen from Eq. (A13) that there is an optimum value of beam thickness which is given by

$$\sigma_1=1.2\ \text{ or }\ a=0.6l/\pi\cong 1.2\nu_0/\omega_r. \tag{A13}$$

It is easy to check that the optimum value of the beam width ($b=0.8r_x$) found above is also optimum for this case. With these values of a and b, we may rewrite expression (A12) in the following form:

$$G\cong\left(\frac{|e|}{m}\right)^{1/2}\frac{W}{c}\frac{0.06J_0Qr_y\lambda}{(q+1/2)\Theta_d U_0^{1/2}}. \tag{A14}$$

The norm of oscillation for this case reads

$$N_r=1.2\varepsilon_0\lambda(q+1/2)r_x r_y\Theta_d. \tag{A15}$$

[1] F. S. Rusin and G. D. Bogomolov, Pis'ma Zh. Eksp. Teor. Fiz. **4**, 236 (1966) [JETP Lett. **4**, 160 (1966)].

[2] V. P. Shestopalov, *Diffraction Electronics* (Kharkov University Press, Kharkov, 1976) (in Russian).

[3] K. Mizuno, S. Ono, and Y. Shibata, IEEE Trans. Electron Devices **92**, 749 (1973).

[4] R. P. Leavitt, D. E. Wortman, and C. A. Morrison, Appl. Phys. Lett. **35**, 363 (1979).

[5] E. M. Marshall, P. M. Phillips, and J. E. Walsh, IEEE Trans. Plasma Sci. **16**, 199 (1988).

[6] S. J. Smith and E. M. Purcell, Phys. Rev. **92**, 1069 (1953).

[7] D. M. Vavriv, O. A. Tretyakov, and A. A. Shmatko, Radiotek. Elek. **24**, 812 (1979) [Radio Eng. Electron. Phys. **24**, 119 (1979)].

[8] A. Gover and P. Sprangle, IEEE J. Quantum Electron. **17**, 1196 (1981).

[9] A. A. Shmatko, O. A. Tretyakov, and D. M. Vavriv, Radiat. Eff. **35**, 193 (1979).

[10] B. A. Belyavsky and M. B. Tseitlin, Radiotek. Elek. **29**, 1171 (1984).

[11] R. P. Leavitt, D. E. Wortman, and H. Dropkin, IEEE J. Quantum Electron. **17**, 1333 (1981).

[12] B. Hafizi, P. Sprangle, and P. Serafim, Phys. Rev. A **45**, 8846 (1992).

[13] G. Faby and K. Schünemann, IEEE Trans. Microwave Theory Tech. **11**, 2043 (1997).

[14] V. P. Shestopalov *et al.*, *Generators of Diffraction Radiation* (Naukova Dumka, Kiev, 1991) (in Russian).

[15] A. Gover and Z. Livni, Opt. Commun. **26**, 375 (1978).
[16] D. M. Vavriv and O. A. Tretyakov, Zh. Tekh. Fiz. **54**, 827 (1984) [Sov. Phys. Tech. Phys. **29**, 490 (1984)].
[17] V. K. Kornienko and V. S. Miroshnitshenko, Izv. Vyssh. Uchebn. Zaved. 93 (1983).
[18] I. A. Ivanchenko, Izv. Vyssh. Uchebn. Zaved. Radiofiz. **39**, 414 (1996).
[19] W. E. Lamb, Jr., Phys. Rev. **143**, 1429 (1964).
[20] M. A. Moiseev and G. S. Nusinovich, Izv. Vyssh. Uchebn. Zaved. Radiofiz. **17**, 1709 (1974) [Radiophys. Quantum Electron. **17**, 1305 (1974)].
[21] A. W. Fliflet *et al.*, Phys. Rev. A **43**, 6166 (1991).
[22] L. A. Vainshtain and V. A. Solntsev, *Super-High-Frequency Electronics* (Soviet Radio, Moscow, 1973) (in Russian).
[23] N. N. Bogoliubov and Yu. A. Mitropolski, *Asymptotic Methods in the Theory of Nonlinear Oscillations* (Gordon and Breach, New York, 1961).
[24] V. A. Solntsev, Zh. Tekh. Fiz. **38**, 109 (1968).
[25] D. M. Vavriv, Atti Della Fondazione Giorgio Ronchi **48**, 481 (1993).
[26] F. S. Rusin, in *High-Power Electronics* (Nauka, Moscow, 1968), Vol. 5, p. 9 (in Russian).
[27] Yu. I. Yevdokimenko *et al.*, Dokl. Akad. Nauk SSSR **265**, 318 (1982).
[28] D. M. Vavriv and Yu. A. Romantsov, Electron. Tekh. Ser. **1**, 3 (1987) (in Russian).
[29] A. A. Andronov and A. L. Fabrikant, in *Nonlinear Waves* (Nauka, Moscow, 1979), p. 68 (in Russian).
[30] R. E. Collin, *Foundations for Microwave Engineering* (McGraw-Hill, New York, 1966).
[31] J. M. Guckenheimer and P. Holms, *Nonlinear Oscillations, Dynamical Systems and Bifurcations of Vector Fields* (Springer, Berlin, 1983).
[32] D. M. Vavriv *et al.*, Phys. Rev. E **53**, 103 (1996).
[33] D. M. Vavriv, Radiotekh. Elektron. **27**, 1576 (1982).
[34] V. L. Bratman, N. S. Ginsburg, and M. I. Petelin, in *Lectures on Microwave Electronics and Radio Physics* (Saratov State University Press, Saratov, 1981), Vol. 1, p. 69.